Journal of Power Sources 223 (2013) 349–357

Contents lists available at SciVerse ScienceDirect

Journal of Power Sources

journal homepage: www.elsevier.com/locate/jpowsour

Influence of the oxygen electrode and inter-diffusion barrier on the degradation of solid oxide electrolysis cells

Per Hjalmarsson*, Xiufu Sun, Yi-Lin Liu, Ming Chen

Department of Energy Conversion and Storage, Technical University of Denmark, Fredrikborgsvej 399, P.O. Box 49, DK-4000 Roskilde, Denmark

HIGHLIGHTS

- ► Two SOECs with LSCF:CGO and LSM:YSZ oxygen electrodes were tested.
- ► The tests were carried out at -1.5 Acm^{-2} and co-electrolysis conditions.
- ► The LSCF electrode was electrochemically more stable than its LSM counterpart.
- ► The electrolyte of the LSCF cell was more stable than that of the LSM:YSZ cell.
- ► The Ni:YSZ electrode was more stable in the cell with an LSCF:CGO electrode.

ARTICLE INFO

Article history:
Received 21 June 2012
Received in revised form
21 August 2012
Accepted 22 August 2012
Available online 25 September 2012

Keywords:
SOEC
Solid oxide electrolysis cell
Co-electrolysis
Electrolysis
Degradation
MIEC

ABSTRACT

Two Solid Oxide Electrolysis Cells (SOECs) with different oxygen electrodes have been tested in galvanostatic tests carried out at -1.5 Acm^{-2} and 800 °C converting 60% of a 50:50% mixture of H_2O and CO_2 (co-electrolysis). One of the cells had an LSM:YSZ oxygen electrode. The other had an CGO inter-diffusion barrier sandwiched between the YSZ electrolyte and an LSCF:CGO oxygen electrode. Impedance Spectroscopy was used during the tests to diagnose the change in electrochemical response of the different components of the SOECs. The results showed a significantly lower degradation rate for the cell with an LSCF:CGO oxygen electrode. This was attributed to three different effects: (1) The LSCF electrode was found to be more stable than its LSM:YSZ based counterpart. (2) The crack propagation in the YSZ electrolyte was less severe in the cell with an LSCF electrode. (3) The Ni:YSZ degradation was less severe in the cell with an LSCF electrode. We hypothesize further that (2) is an effect of the CGO inter-diffusion layer and that (3) is an indirect effect of (2).

1. Introduction

Solid oxide electrolysis cells (SOECs) offer a promising technology for efficient energy conversion and production of hydrogen or syngas (mixture of H_2 and CO) using excess electrical energy from renewable energy sources such as wind or solar energy [1–4]. Synthetic liquid fuels possess higher volumetric energy density as compared to hydrogen and can be easily stored, transported and consumed based on current infrastructure [1–5]. Therefore, from a storage point of view, co-electrolysis of $H_2O + CO_2$ is more attractive as compared to steam electrolysis, as the produced syngas can be catalysed further into various types of synthetic fuels such as ethanol, dimethyl ether (DME) or synthetic diesel.

In order to reach commercialization it is important to increase the expected operational lifetime to at least 5 years [5,6]. In recent years the degradation of SOECs has therefore been extensively studied under various conditions incl. steam electrolysis [7–10], CO_2 electrolysis [11] or co-electrolysis [12,13]. A number of different degradation mechanisms have been proposed such as segregation of impurity phases to the triple phase boundary (TPB) [10], poisoning of the electrodes by impurities from the gas stream [13] and oxygen electrode delamination due to large oxygen activity gradients [7,9,14]. At current densities below 1 A cm^{-2}, it has been argued that impurity poisoning of the Ni:YSZ TPBs is the main cause for degradation.

For the SOEC technology to become commercially competitive it is beneficial to operate the cells at high current densities in order to decrease both investment and production costs. However, at current densities $\geq$1 A cm^{-2} it has been reported that lateral cracks forms within the 8% Y_2O_3 stabilised ZrO_2 (YSZ) electrolyte causing

* Corresponding author. Tel.: +45 4677 5759; fax: +45 4677 5758.
E-mail addresses: phja@dtu.dk, phja@risoe.dtu.dk (P. Hjalmarsson).

0378-7753/$ – see front matter © 2012 Elsevier B.V. All rights reserved.
http://dx.doi.org/10.1016/j.jpowsour.2012.08.063

an additional, and rather severe, degradation process. [7] It was observed that inter-granular nano-pores had formed within YSZ close to the LSM:YSZ ($La_{1-x}Sr_xMnO_3$) oxygen electrode. This weakens the electrolyte to such a degree that cracks start to propagate laterally within the YSZ. The authors of the aforementioned study argued this to be an effect of high oxygen potentials on this side of the cell during strong electrolysis polarization. The study was carried out on cells with identical LSM:YSZ electrodes, thus did not reveal whether this degradation process is also dependent on the overpotential of the oxygen electrode.

During the last ten years $La_{1-x}Sr_xCo_{1-y}Fe_yO_{3-\delta}$ (LSCF) has emerged as an alternative material for oxygen electrodes in Solid Oxide Cells (SOC). LSCF is a mixed electronic and ionic conducting material (MIEC) yielding better transport properties and lower polarisation resistance as compared to that of the LSM:YSZ electrode [15]. Unfortunately, LSCF is known to react with YSZ at the temperatures were SOECs are manufactured and operated, leaving electrically insulating phases of $SrZrO_3$ and $La_2Zr_2O_7$ as products [16]. For this reason it is necessary to apply an inter-diffusion barrier layer between the YSZ electrolyte and the LSCF based electrode preventing the reaction. The effect of such a bi-layer electrolyte is that the detrimentally higher oxygen potential will be found within the inter-diffusion barrier consisting of a different material and microstructure. It is therefore of interest, from both a scientific and technological point of view, to study the degradation of SOECs having a CGO inter-diffusion barrier and an LSCF based electrode.

2. Experimental

Two anode supported SOECs were manufactured using identical half cells consisting of a support (Ni:3YSZ cermets), a fuel electrode (Ni:8YSZ cermets) and an electrolyte (8YSZ). An LSM:YSZ oxygen electrode was screen printed onto the cells hereafter referred to as Cell A1 and A2, where A2 is the reference cell. A CGO10 inter-diffusion layer and LSCF:CGO oxygen electrode were sequentially applied onto the cells hereafter referred to as Cell B1 and B2, where B2 is the reference cell.

The cells were tested in a SOFC test setup described elsewhere [17]. Steel spacers and glass felt with glass softening and glass transition temperatures of approximately 670 °C and 790 °C respectively were used to seal the anode and cathode gas flow compartments. Gold and Nickel meshes were used as current collector components on the oxygen and fuel side, respectively. Eight kilograms of weight was applied on top of the cell house during start up to ensure gas tight sealants and electrical contact between the cell and the contact components. The flow compartments were sealed at 850 °C for 2 h prior to fuel electrode reduction. The fuel electrode was reduced in 9% H_2 in N_2 for 2 h followed by 1 h in humidified H_2 (4% H_2O).

The electrochemical characteristics of the cells were tested at 850 °C, 800 °C and 750 °C. At each temperature i–v polarization and EIS measurements were carried out with both air and O_2 supplied to the oxygen electrode and with a steam content of both 20% and 50% supplied to the anode side. Flows were set to 50 lh^{-1} of air/O_2 and 24 lh^{-1} of H_2/H_2O. i–v polarization measurements were carried out under co-electrolysis condition with a 24 lh^{-1} flow of oxidants ($x^{CO2}_{Ni:YSZ} = 0.45$, $x^{H2O}_{Ni:YSZ} = 0.45$, $x^{H2}_{Ni:YSZ} = 0.1$) and with 50 lh^{-1} O_2 supplied to the oxygen electrode. EIS measurements were carried out at zero net current using a Solartron 1255 frequency analyzer and an external shunt resistor in series with the cell. The initial electrochemical performance of nominally identical reference cells, Cell A2 and Cell B2, was tested accordingly. All cells were cooled to room temperature in 9% H_2 in N_2 on the fuel electrode side after test.

The electrochemical stability of Cell A1 and Cell B1 when operated in co-electrolysis was tested in galvanostatic experiments carried out at −1.5 A cm^{-2} and 800 °C with an oxidant utilisation of 62%. The oxidant molar fraction was set to $x^{CO2}_{Ni:YSZ} = 0.45$, $x^{H2O}_{Ni:YSZ} = 0.45$, $x^{H2}_{Ni:YSZ} = 0.1$. The 10% of hydrogen excess was added in order to avoid too oxidizing atmospheres at the fuel electrode inlet. All gas supplied to the Ni:YSZ electrode were cleaned at 750 °C before being fed to the cell, following the procedure described by Ebbesen et al. [13].

A flow of 50 l h^{-1} of O_2 was supplied to the oxygen electrode in order to ensure a stable P_{O2} along the oxygen electrode area. EIS measurements were recorded throughout the tests. The electrochemical characteristics of both cells were tested afterwards according to the same protocol as prior to the galvanostatic test. The electrochemical characteristics of Cell A2 and B2 were similar to that of Cell A1 and Cell B1 respectively and were primarily used for assessing microstructural changes induced by the galvanostatic tests of Cell A1 and Cell B1. In this study, analysis of the impedance data was performed using impedance transforms in the software Ravdav [18]. Cell A1 was first tested for 60 h at −1 Acm^{-2}, which was considered as a short period of no interest and importance in the context of this publication. Some of the results from test of Cell A1, analysed in less detail and with a different scope, was reported in Ref. [19].

For microstructural examination, polished cross-section of all cells were prepared. A Carl Zeiss Supra 35 scanning electron microscope (SEM), equipped with a field emission gun (FEG) and an Energy Dispersive Spectrometer (EDS) was used. The samples were carbon coated prior to imaging and EDS analysis which was carried out at an accelerating voltage of 14 kV. Percolation analysis of Ni was studied using non-carbon coated samples and an accelerating voltage of 0.95 kV [20]. EDS data was analysed using an x-ray microanalysis software NSS from Thermo Fischer Scientific INC.

3. Results

Fig. 1 plots the results from i–v polarization measurements of Cell A and Cell B recorded at 800 °C under co-electrolysis conditions before and after the durability tests. The results show that Cell B has lower initial resistance than Cell A. The secant resistance at 1250 mV was calculated to have increased from 0.31 to 0.57 Ω cm^2 for Cell A Ω cm^2 and from 0.27 to 0.41 Ω cm^2 for Cell B.

Fig. 2 plots cell voltage curves of the galvanostatic tests of Cell A1 and Cell B1. The voltage fluctuation during the initial 75 h of the

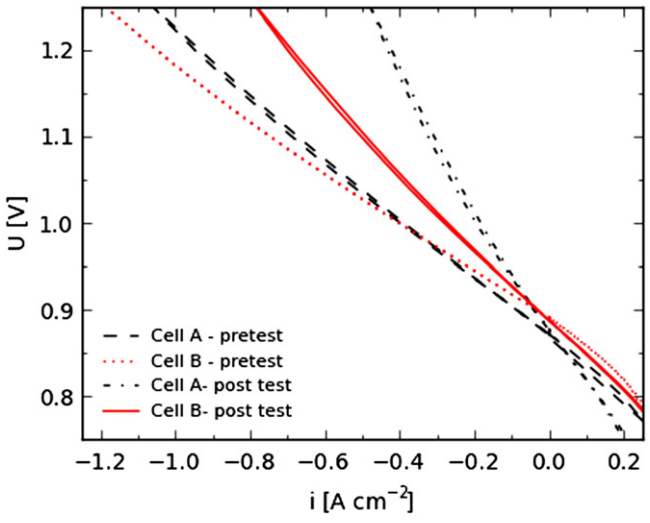

Fig. 1. I–V polarization measurements of Cell A and Cell B at 800 °C measured under co-electrolysis condition before and after the durability tests.

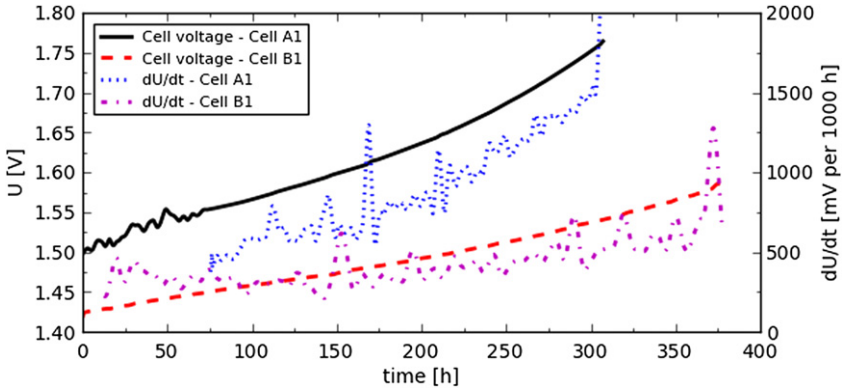

Fig. 2. Galvanostatic (−1.5 A cm^2) cell voltage curves measured at 800 °C under co-electrolysis flows described in the experimental section.

test of Cell A1 was caused by an unstable supply of steam. This problem was resolved by heat isolation of the steam supply line in order to prevent condensation. The figure plots further the time derivative of the cell voltage from which it is apparent that the degradation rates of both Cell A1 and Cell B1 increase with time. For Cell A1 the degradation rate increased from about 500 to 1500 mV kh^{-1} whereas the degradation rate of Cell B1 increased from about 300 to 600 mV kh^{-1} during the test.

EIS measurements were recorded throughout the galvanostatic tests. The impedance spectra were analysed using the following constant linear least square (CNLS) models: L-R_S-$(RQ)_{EL}$-$(RQ)_{EL}$-G_{EL}-$(RQ)_{DIFF}$ -$(RC)_{CONV}$ where $(RQ)_{EL}$ and G_{EL} (Gerischer) represents electrochemical processes associated with the two electrodes [21]. Fig. 3 simulates, for a representative impedance spectra measured during the test of Cell B1, the different elements of the model. It also compares modelled and measured impedance data in a residual error plot. The equivalent circuit elements representing electrode processes were clearly discriminated from those representing gas diffusion and conversion impedances. However, it was not possible to distinguish with certainty the elements associate with the cathode and anode processes due to frequency overlap of the different electrode processes. Therefore trends in the resistance of the individual processes could not be adequately and satisfactorily determined using the method of CNLS fitting. Instead, Fig. 4 plots the increase in total resistance associated with the two electrodes, i.e. $(RQ)_{DIFF}$ and $(RC)_{CONV}$ subtracted from the polarization resistance (R_P). Fig. 4 plots also the increase in serial resistance of Cell A1 and Cell B1. The results from the impedance measurements show that both the resistance associated with the electrolyte and the electrodes increase faster for Cell A1 than Cell B1.

Furthermore, it can be concluded that the degradation rate of both the cell voltage and R_S increased throughout the test. The correlation between the apparently accelerated increase in cell voltage and R_S was found for both Cell A1 and Cell B1 though the acceleration appears to be stronger for Cell A1 as compared to Cell B1. In contrast, R_P of both Cell A1 and B1 were found to increase

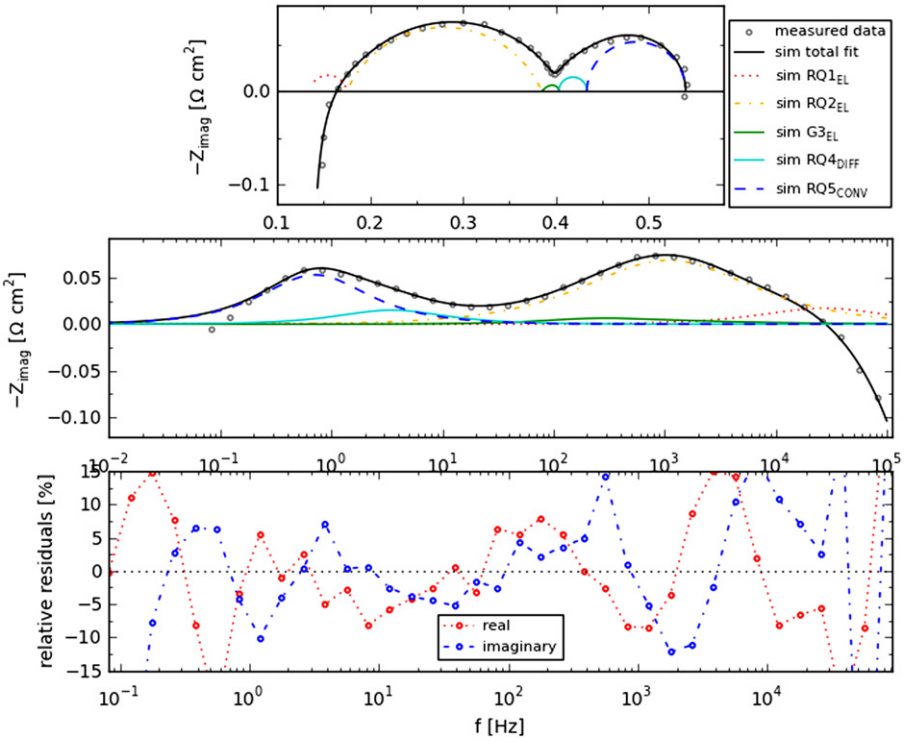

Fig. 3. Simulation and error plot of the CNLS model used to fit impedance data measured during test, in this case that of Cell B1.

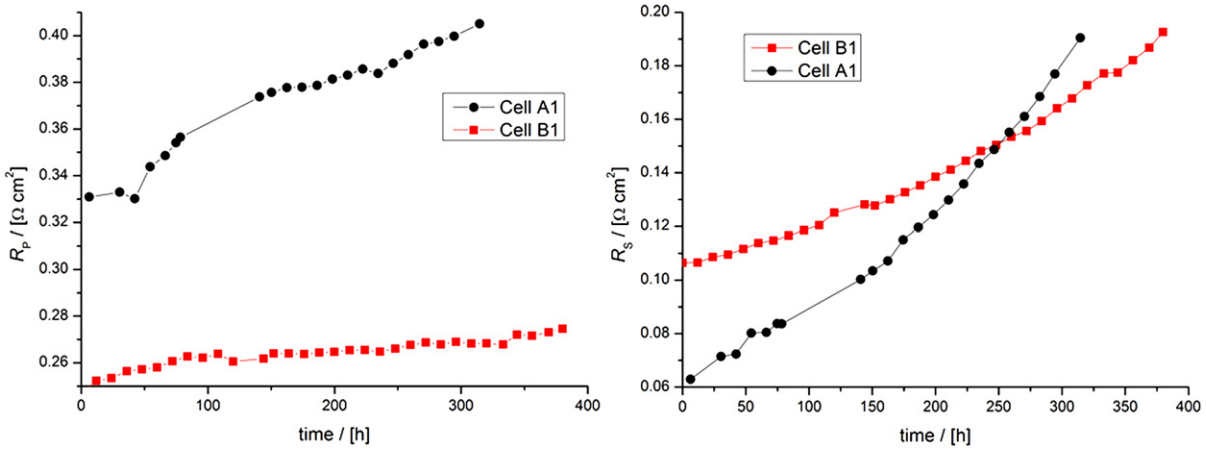

Fig. 4. Left: The electrochemical part of the polarisation resistance (left figure) and serial resistance (right figure) extracted from EIS recorded during the galvanostatic tests reported in Fig. 2.

approximately linearly throughout the test. The degradation rate for R_P of Cell A1 was calculated to 235 mΩ cm^2 kh^{-1} whereas the corresponding rate for Cell B1 was found to be 74 mΩ cm^2 kh^{-1}.

Impedance spectra measured before and after testing were analysed using the method of analysis of difference in impedance spectra (ADIS) [22]. The method is limited to analyse electrode reactions that have a partial pressures dependence of the respective reactants and products. This is the case for most of the electrochemical processes occurring in a SOEC. By applying the ADIS methodology it is possible to determine a change in the impedance response at a given frequency upon a shift in either P_{H2O} or P_{O2} on the fuel or oxygen electrode side respectively. A stronger ADIS response after test for a given electrode can then be interpreted as an increase in resistance for this specific electrode reaction. Such an interpretation assumes that the partial pressure dependence of the electrodes does not change during the test. This is a reasonable assumption.

Gas shift ADIS analysis was used in order to analyse impedance spectra recorded before and after the durability tests. The results are plotted in Figs. 5 and 6 for Cell A1 and Cell B1. Significant changes in the ADIS response was observed for both electrodes of Cell A1 indicating that both the Ni:YSZ and the LSM:YSZ electrodes had degraded during the test. The change was particularly strong for the Ni:YSZ electrode implying that most of the electrode degradation had occur on this side of the cell. Moreover, a significant shift of the summit frequency from about 5 kHz to 500 Hz was observed.

Results from the ADIS analysis of Cell B1 showed significant differences to that of Cell A1. Firstly, the change in the ADIS response of the Ni:YSZ electrode was much weaker for Cell B1 than Cell A1. This indicates that the nickel electrode had degraded to a substantially larger degree in Cell A1 than in Cell B1, despite that they are identical and have been tested under the same conditions. Secondly, no change in the ADIS response of the oxygen electrode

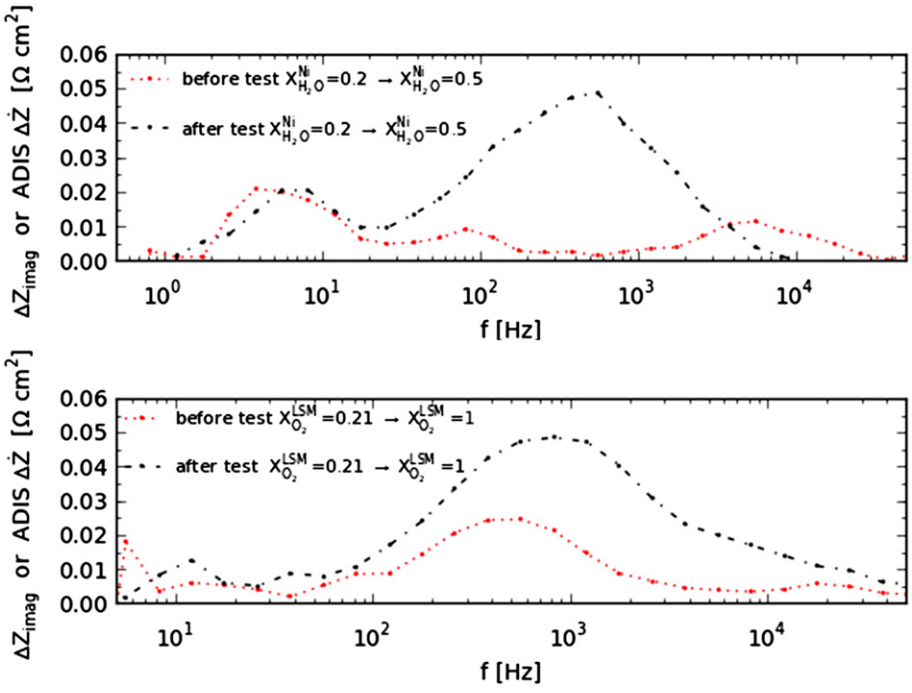

Fig. 5. Steam shift (top figure) and oxygen shift (bottom figure) ADIS analysis of Cell A1 before and after the galvanostatic test.

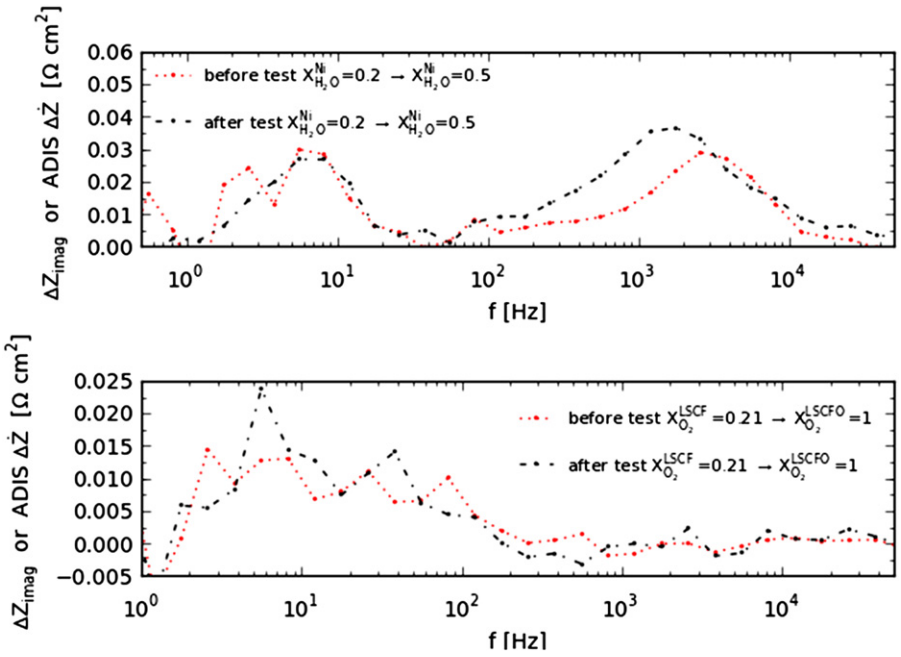

Fig. 6. Steam shift (top figure) and oxygen shift (bottom figure) ADIS analysis of Cell B1 before and after the galvanostatic test.

(LSCF:CGO) could be observed. A weak peak in the ADIS analysis is found at 10–100 Hz, which is the typical frequency regime for MIEC electrode. The results indicate that the LSCF:CGO electrode does not degrade during the galvanostatic test, in contrast to that occurring at the LSM:YSZ. It should be noted in this context that this method can only be used to distinguish changes in electrode processes that have a dependency on P_{H2O} or P_{O2}.

The impedance recorded during the galvanostatic tests were analysed using the methodology distribution of relaxation times (DRT) [23]. Applying DRT to measured impedance data allows to distinguish, with high resolution, the frequencies at which the resistance of a process increase or decrease upon a change in condition (P_X, T, i, η, time etc). Fig. 7 plots the results of the DRT analysis of Cell A1 and Cell B1 during the test and shows an increase in the main electrode response at around 1 kHz during the first approximate 150 h of the test of Cell A1. Additionally, the summit frequency of this process appears to shift from about 2 to 1 kHz. It is known from previous studies and from the ADIS analysis that the electrochemical processes at the Ni:YSZ electrode occurs within this frequency regime [12]. Consequently, this process is hereafter ascribed to the fuel electrode. Fig. 7 shows further that the electrochemical response of the Ni:YSZ electrode of Cell B1, which is identical to that of Cell A1, does not seem to increase in magnitude. A shift towards lower frequencies, similar to that seen for Cell A1,

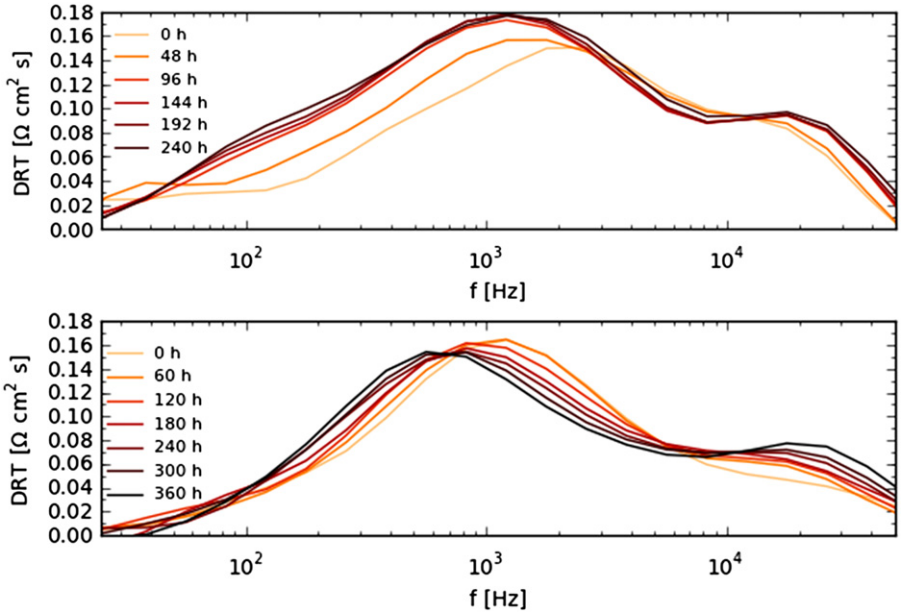

Fig. 7. Change in polarisation resistance during the galvanostatic tests of Cell A1 (top figure) and Cell B1 (bottom figure) when analysed using the method of distribution of relaxation times (DRT).

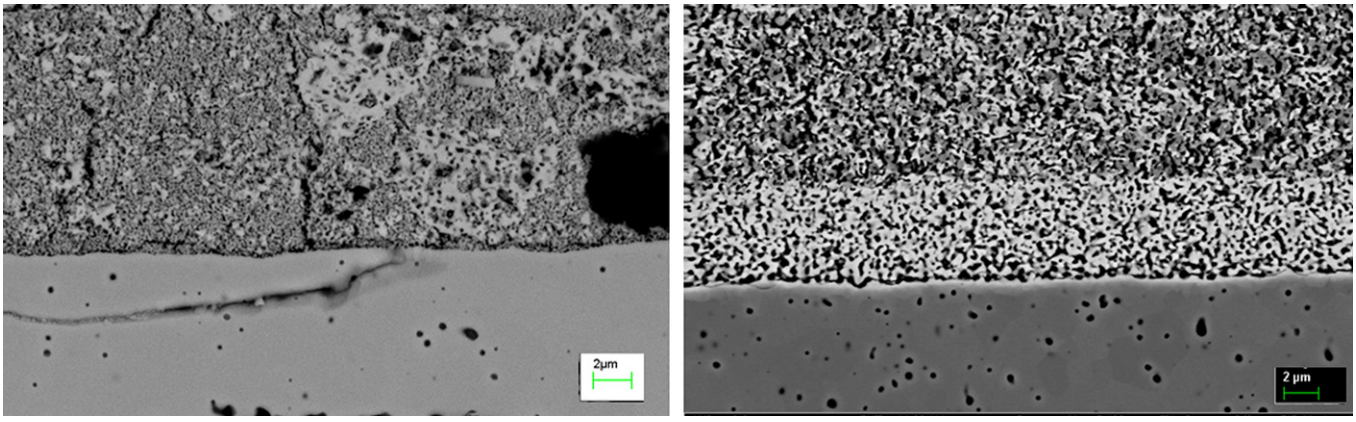

Fig. 8. Micrographs of Cell A1 (top left) and Cell B1 (right) showing the typical microstructure of the oxygen electrode, CGO inter-diffusion barrier (Cell B1) and the YSZ electrolyte.

was also observed for Cell B1. This shift was also observed in the ADIS analysis. The increase in electrode resistance observed for Cell B1 in Fig. 4 appears instead to be related to a response occurring at frequencies around 20–30 kHz.

Fig. 8 shows micrographs of the electrolytes and the oxygen electrodes of Cell A1 and Cell B1 after test. Horizontal cracks within the YSZ electrolyte of Cell A1 were found throughout the sample. No such cracks were observed in neither Cell B1 nor in any of the reference cells.

Fig. 9 shows micrographs of the active cathode and the Ni:YSZ support of Cell A1, Cell A2 and Cell B1 detected using In-lens secondary electron detector and low accelerating voltage of 0.95 kV [20]. Brighter particles are percolating Nickel whereas darker ones are either non-percolating nickel or YSZ. The micrographs strongly indicate that the degree of nickel percolation has decreased substantially in Cell A1 during the galvanostatic test. Also Cell B1 appears to have lost percolation during the test, however to a significantly lower degree than Cell A1 despite that Cell B1 was tested for a longer period. Furthermore, it can be observed that the nickel particles have coarsened during the tests of Cell A1 and Cell B1. With respect to particles coarsening, no clear difference between Cell A1 and Cell B1 was observed.

Fig. 10 shows micrographs of the active fuel electrode and the Ni:YSZ support of Cell A1, Cell A2 and Cell B1 detected using back-scattered electrons and high accelerating voltage of 15 kV. From the micrographs of Cell A1 thin areas of dark contrast at the Ni:Ni and Ni:YSZ interfaces can be observed. Such features were much less common for Cell B1 and not observed at all in the reference Cell A2.

Fig. 11 shows backscatter micrographs of the CGO:YSZ interface of Cell B1 and Cell B2. From the micrograph of Cell B1 cracks at the interface between the CGO particles and the YSZ electrolyte are observed. These cracks cannot be seen in the micrographs of Cell B2 indicating that this interface appears to have been weakened during the galvanostatic test. Underneath the inter-diffusion barrier, a reaction zone with a depth of about 1 µm can be observed. EDS line scan analysis, shown in Fig. 12, reveal that this

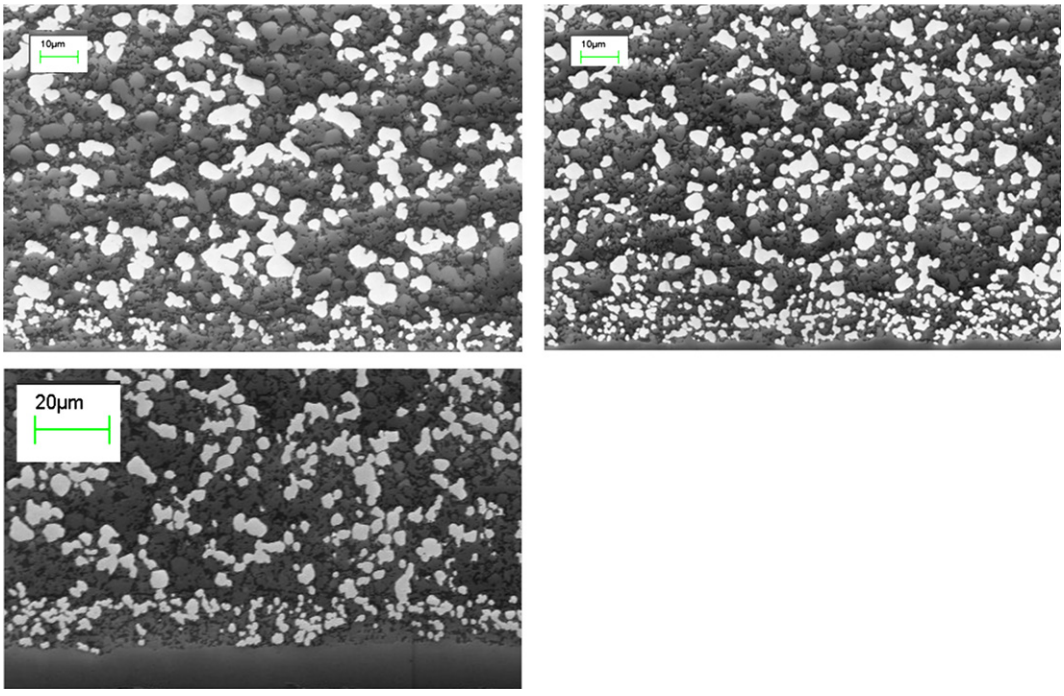

Fig. 9. Low voltage secondary electron micrographs of Ni:YSZ cathode of Cell A1 (top left), Cell A2 (top right) and Cell B1 (bottom left).

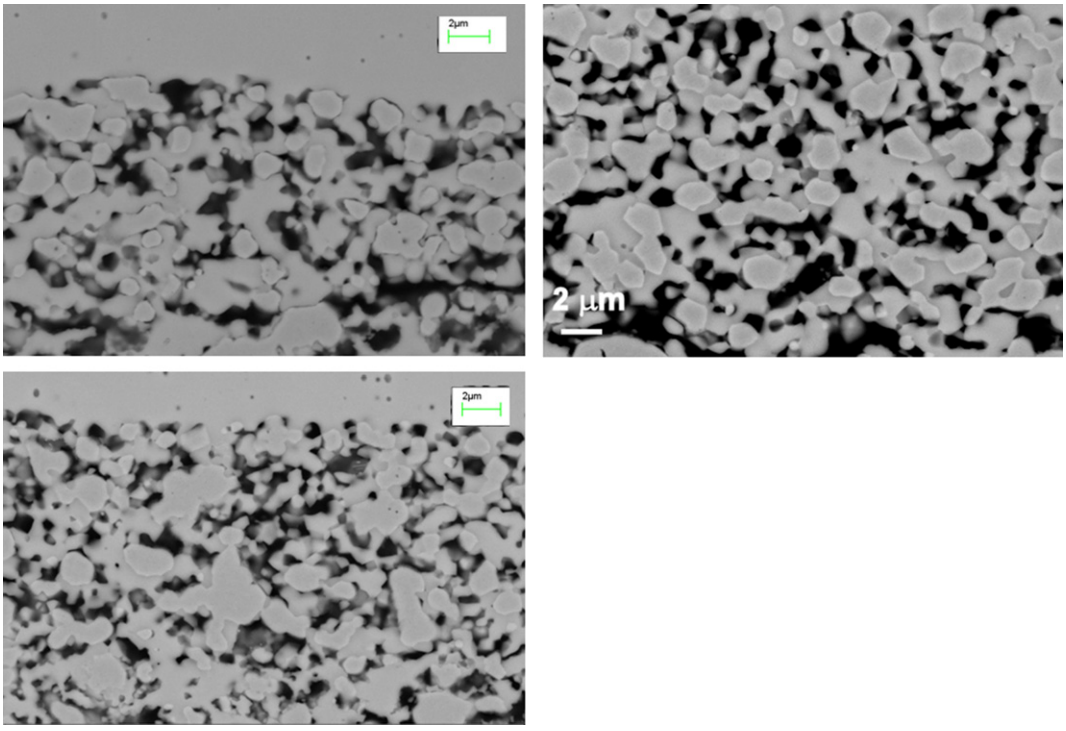

Fig. 10. SEM back-scattered micrographs of Ni:YSZ cathodes of Cell A1 (top left), Cell A2 (top right) and Cell B1 (bottom left).

layer consist of a CGO:YSZ inter-diffusion layer. Small traces of less than 4 At% of Sr was also found just beneath the CGO inter-diffusion layer. No difference in the extent and depth of the reaction layer can be confirmed between Cell B1 and Cell B2.

4. Discussion

The lower initial resistance of Cell B1 compared to Cell A1 as measured by *i*–*v* polarization agree well with results from testing SOFCs with LSM and LSCF based oxygen electrodes [24]. Detailed analysis of the initial performance of these cell types has been reported in earlier papers and will not be discussed in further detail here [25,26]. However, the *iv*-curves showed also that Cell B1 was substantially more stable as the secant ASR increase about only about 50% as compare to the almost doubling of the ASR measured for Cell A1. The difference in stability between Cell A1 and Cell B1 was also confirmed from the measured cell voltage and impedance spectroscopy data during the galvanostatic tests.

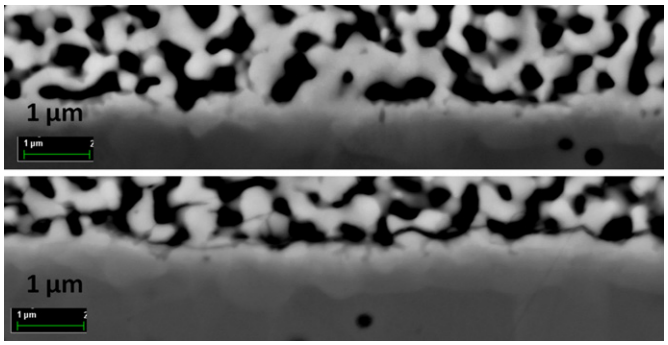

Fig. 11. Backscatter micrographs of the interface between the YSZ electrolyte and the CGO inter-diffusion barrier of Cell B1 (bottom) and Cell B2 (top).

The results from the impedance measurements, recorded in situ during the galvanostatic tests, indicate that cell voltage degradation is mainly associated with an increase in the serial resistance. This is supported not only by the accelerated degradation seen for both cell voltage and R_S but also by the fact that R_S increases substantially more than R_P. A plausible reason for the increase in R_S when operating the SOEC at high current densities was discussed by Knibbe et al. [7]. The authors argued that the oxygen potential increases on the oxygen side of the cell to such high levels that gaseous oxygen form within the fraction of the electrolyte closest to the oxygen electrode. The oxygen dissolution results in the formation of small porosities (~30 nm) at the grain boundaries, which eventually weakens that interface to the extent that inter-granular fractures start to form.

Fractures, similar to those found in the aforementioned study, were also observed within the YSZ electrolyte of Cell A1. As Cell A1 is identical to those reported by Knibbe et al. and was tested under the same current load, it is therefore reasonable to assume that the increase in R_S of Cell A1 is related to the same phenomenon. For Cell B1 no such fractures were found. Instead, cracks at the CGO:YSZ interface were seen throughout the sample. These cracks were not observed in Cell B2 which suggests that the cracks had formed during the test. This could possibly indicate that the above discussed nano-porosity have formed at the grain boundaries between the CGO and YSZ particles in Cell B1. However, the grain boundary porosity and subsequent inter-granular cracks should, according to the aforementioned authors, occur close to the oxygen electrode, where the oxygen potential is the highest, and not at the CGO:YSZ interface.

Small traces of strontium was found below the inter-diffusion barrier but the concentration was so low that it is high unlikely that $SrZrO_3$ formation caused the increase in R_S of Cell B. The solid solution of CGO and YSZ, known form above 1200 °C, was found to approximately the same extent in both Cell B1 and B2. We therefore conclude that it was formed during sintering of the CGO inter-diffusion barrier [27]. Solid solution of YSZ and CGO has

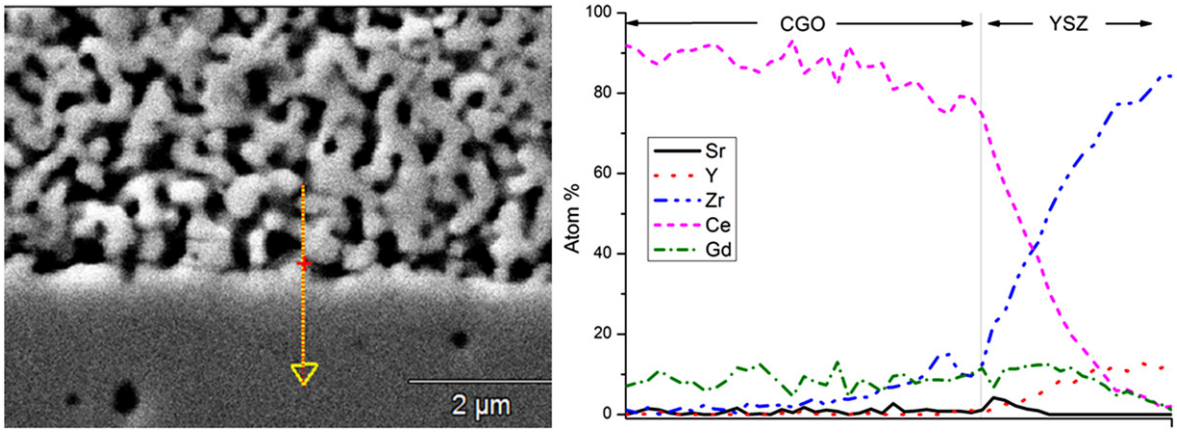

Fig. 12. EDS line scan across the CGO:YSZ interface of Cell B1.

substantially lower ionic conductivity as a result of trapping of oxygen vacancies and increased lattice strain due to differences in ionic radius of Ce^{4+} and Zr^4 [28–30]. Additionally, the high degree of CGO porosity at the interface introduces further geometric constrains for oxygen ion transfer across the YSZ:CGO interface. These two effects may lead to significant overpotentials across the thin layer of YSZ:CGO solid solution. Additionally, the YSZ:CGO interface is a mechanical weak point due to non-ideal sintering and lattice mismatch between YSZ and CGO particles where the constrained CGO layer sintering leads to a relatively high porosity. Furthermore, the solid solution of CGO and YSZ leads to an increase in the thermal expansion coefficient which will introduce further stresses at the interface potentially leading to fracture over time [30]. It could therefore be that the fracture at the CGO:YSZ interface has arisen as of a different cause than for Cell A1. To further elucidate whether the fractures at the CGO:YSZ interface is primarily caused by a mechanical or electrochemical degradation mechanism more systematic studies changing the porosity and the extent of solid solution are required.

A possible consequence of the CGO inter-diffusion barrier is thus that it effectively places the detrimentally high oxygen potential outside the YSZ electrolyte. The fact that R_S of Cell B1 degraded less than R_S of Cell A1 suggests further that a fracture at this interface is less detrimental to the serial resistance. Moreover, if the increase in R_S of Cell B1 is related to manufacturing of the inter-diffusion barrier, rather than nature of the YSZ grains and the oxygen potential at high cell voltage, this degradation problem can possibly be circumvented by an improved cell design.

DRT analysis of impedance spectra measured during test as well as ADIS analysis of impedance measured before and after test showed that most of electrode degradation in Cell A1 is associated with the Ni:YSZ electrode. Furthermore, microstructural analysis of the Ni:YSZ electrode suggests that the degradation is, at least partially, correlated to loss of Ni percolation as a result of insulting phases at the grain boundaries [19]. Traces of silica are known to be present both in the sealant and as an impurity in the raw material from which the cells are made. Silica is believed to be transported in the form of $Si(OH)_4$ to the TPB at which it's undergoes the reaction: $Si(OH)_4 \rightarrow SiO_2 + 2H_2O$ [31]. A high local overpotential and current density will shift the reaction to the right favoring the transport to, and deposition of Si at the Ni:YSZ TPB.

Interestingly, it was observed that R_P of Cell B1 did not degrade to the same degree as for Cell A1. This was partially due to the fact that the LSCF based oxygen electrode appears to be more stable than its LSM based counterpart. Similar results have been obtained previously on anode supported SOFCs where LSCF based cathodes have shown higher stability, especially under moisturized air flow. The authors argued that the higher electrochemical stability of LSCF was to be an effect of its MIEC property spreading out the current distribution and thus overpotential over a much larger area than only at the triple phase boundaries [32]. However, the ADIS analysis showed also a significant difference in the extent of degradation on the Ni:YSZ electrode. This finding was supported further by microstructural analysis showing a substantially larger degree of Ni percolation and much lower degree of secondary phases at the grain boundaries in Cell B1 than in Cell A1.

Since the Ni:YSZ electrodes and the YSZ electrolytes of Cell A1 and Cell B1 are identical, this difference could only be explained as an indirect effect of the oxygen electrode and the presence of an inter-diffusion barrier. As already discussed in this paper, operating a cell with an LSM:YSZ electrode results in lateral cracks within the electrolyte. This will passivate the fraction of the cell area within which these cracks have propagated, in turn leading to a smaller active cell area. The consequence is that the effective current density of the still active areas of the cell is even higher than the apparent 1.5 A cm^{-2} resulting in even high overpotential and driving force for deposition of SiO_2 segregation to the still active Ni:YSZ TPB. Additionally, high local over-potential at the Ni:YSZ TPB may increase the driving forces and rates for other detrimental electrochemical degradation processes such as reduction of YSZ.

5. Conclusion

Degradation of two SOECs with different oxygen electrodes has been studied at −1.5 Acm^{-2}, 800 °C and 62% conversion of a 50:50% H_2O:CO_2 mixture (co-electrolysis). The first cell had an LSM:YSZ oxygen electrode. The second cell had an CGO inter-diffusion barrier sandwiched between the YSZ electrolyte and an LSCF:CGO oxygen electrode. The results showed a lower overall degradation for the cell with an LSCF:CGO oxygen electrode. Analysis of measured impedance spectroscopy data found that the LSCF electrode was electrochemically more stable than its LSM:YSZ based counterpart. However, the main reason for the lower degradation rate was an electrochemically more stable bi-layer electrolyte. We hypothesize that the use of an inter-diffusion barrier and an electrochemically more active oxygen electrode reduces the oxygen potential within the YSZ electrolyte, which in turn reduces the formation of inter-granular cracks within the YSZ that otherwise tend to show up under high polarisation. We hypothesize further that there is a correlation between the stability of the YSZ electrolyte and the Ni:YSZ fuel electrode when the SOEC is operated at high current densities.

References

[1] S.H. Jensen, P.H. Larsen, M. Mogensen, Int. J. Hydrogen Energy 32 (2007) 3253–3257.
[2] Z. Zhan, W. Kobsiriphat, J.R. Wilson, M. Pillai, I. Kim, S.A. Barnett, Energy Fuels 23 (2009) 3089–3096.
[3] S.D. Ebbesen, C. Graves, M. Mogensen, Int. J. Green Energy 6 (2009) 646–660.
[4] J. Hartvigsen, S. Elangovan, L. Frost, A. Nickens, C. Stoots, J. O'Brien, J.S. Herring, Fuel Cell Seminar 2007, 12 (2008) 625–637.
[5] C. Graves, S.D. Ebbesen, M. Mogensen, K.S. Lackner, Renewable Sustain. Energy Rev. 15 (2011) 1–23.
[6] Q. Fu, C. Mabilat, M. Zahid, A. Brisse, L. Gautier, Energy Environ. Sci. 3 (2010) 1382–1397.
[7] R. Knibbe, M.L. Traulsen, A. Hauch, S.D. Ebbesen, M. Mogensen, J. Electrochem. Soc. 157 (2010) B1209–B1217.
[8] G. Schiller, A. Ansar, M. Lang, O. Patz, J. Appl. Electrochem. 39 (2009) 293–301.
[9] M.A. Laguna-Bercero, R. Campana, A. Larrea, J.A. Kilner, V.M. Orera, J. Power Sources 196 (2011) 8942–8947.
[10] A. Hauch, S.D. Ebbesen, S.H. Jensen, M. Mogensen, J. Electrochem. Soc. 155 (2008) B1184–B1193.
[11] S.D. Ebbesen, M. Mogensen, J. Power Sources 193 (2009) 349–358.
[12] C. Graves, S.D. Ebbesen, M. Mogensen, Solid State Ionics 192 (2011) 398–403.
[13] S.D. Ebbesen, C. Graves, A. Hauch, S.H. Jensen, M. Mogensen, J. Electrochem. Soc. 157 (2010) B1419–B1429.
[14] A.V. Virkar, Int. J. Hydrogen Energy 35 (2010) 9527–9543.
[15] F.S. Baumann, J. Fleig, G. Cristiani, B. Stuhlhofer, H.U. Habermeier, J. Maier, J. Electrochem. Soc. 154 (2007) B931–B941.
[16] C.C. Chen, M.M. Nasrallah, H.U. Anderson, J. Electrochem. Soc. 140 (1993) 3555–3560.
[17] P.V. Hendriksen, M. Mogensen (2003) 261.
[18] C. Graves, RAVDAV Data Analysis Software, 0.9.7 (2012).
[19] X. Sun, M. Chen, P. Hjalmarsson, S.D. Ebbesen, S.H. Jensen, M. Mogensen, P.V. Hendriksen, ECS Trans. 41 (2012) 77–85.
[20] K. Thyden, Y.L. Liu, J.B. Bilde-Sorensen, Solid State Ionics 178 (2008) 1984–1989.
[21] A. Leonide, V. Sonn, A. Weber, E. Ivers-Tiffe, J. Electrochem. Soc. 155 (2008) B36–B41.
[22] S.H. Jensen, A. Hauch, P.V. Hendriksen, M. Mogensen, N. Bonanos, T. Jacobsen, J. Electrochem. Soc. 154 (2007) B1325–B1330.
[23] H. Schichlein, A.C. Muller, M. Voigts, A. Krugel, E. Ivers-Tiffee, J. Appl. Electrochem. 32 (2002) 875–882.
[24] A. Mai, V.A.C. Haanappel, S. Uhlenbruck, F. Tietz, D. StÃver, Solid State Ionics 176 (2005) 1341–1350.
[25] R. Barfod, M. Mogensen, T. Klemensø, A. Hagen, Y. Liu, P.V. Hendriksen, J. Electrochem. Soc. 154 (2007) B371–B378.
[26] A. Leonide, B. Rüger, A. Weber, W.A. Meulenberg, E. Ivers-Tiffee, J. Electrochem. Soc. 157 (2010) B234–B239.
[27] A. Tsoga, A. Naoumidis, D. Stover, Solid State Ionics 135 (2000) 403–409.
[28] J.A. Kilner, Solid State Ionics 129 (2000) 13–23.
[29] G. Balducci, J. KaÅ¡par, P. Fornasiero, M. Graziani, M.S. Islam, J.D. Gale, J. Phys. Chem. B 101 (1997) 1750–1753.
[30] X. Zhou, B. Scarfino, H.U. Anderson, Solid State Ionics 175 (2004) 19–22.
[31] A. Hauch, S.H. Jensen, J.B. Bilde-Sorensen, M. Mogensen, J. Electrochem. Soc. 154 (2007) A619–A626.
[32] J. Nielsen, A. Hagen, Y.L. Liu, Solid State Ionics 181 (2010) 517–524.